Time-dependent density functional theory for open systems with a positivity-preserving decomposition scheme for environment spectral functions

RuLin Wang,[1] Xiao Zheng,[2,3,a)] YanHo Kwok,[4] Hang Xie,[4] GuanHua Chen,[4] and ChiYung Yam[1,4,b)]

[1]*Beijing Computational Science Research Center, No. 3 He-Qing Road, Beijing 100084, China*
[2]*Hefei National Laboratory for Physical Sciences at the Microscale, University of Science and Technology of China, Hefei, Anhui 230026, China*
[3]*Synergetic Innovation Center of Quantum Information and Quantum Physics, University of Science and Technology of China, Hefei, Anhui 230026, China*
[4]*Department of Chemistry, The University of Hong Kong, Pokfulam Road, Hong Kong, China*

Understanding electronic dynamics on material surfaces is fundamentally important for applications including nanoelectronics, inhomogeneous catalysis, and photovoltaics. Practical approaches based on time-dependent density functional theory for open systems have been developed to characterize the dissipative dynamics of electrons in bulk materials. The accuracy and reliability of such approaches depend critically on how the electronic structure and memory effects of surrounding material environment are accounted for. In this work, we develop a novel squared-Lorentzian decomposition scheme, which preserves the positive semi-definiteness of the environment spectral matrix. The resulting electronic dynamics is guaranteed to be both accurate and convergent even in the long-time limit. The long-time stability of electronic dynamics simulation is thus greatly improved within the current decomposition scheme. The validity and usefulness of our new approach are exemplified via two prototypical model systems: quasi-one-dimensional atomic chains and two-dimensional bilayer graphene. © *2015 AIP Publishing LLC.* [http://dx.doi.org/10.1063/1.4917172]

I. INTRODUCTION

Understanding nonequilibrium electron dynamics is crucial to the design of novel materials and devices. As an excellent compromise between accuracy and computational cost, time-dependent density functional theory (TDDFT) has been one of the most commonly used theoretical tools in various research areas.[1–4] The Runge-Gross theorem proves the existence of rigorous TDDFT.[1] Despite of its success, conventional TDDFT applies mainly to isolated or periodic systems. Many current research areas involve systems with open boundaries. The existence of a rigorous TDDFT for open electronic systems has been proved based on the time-dependent holographic electron density theorem.[5,6] Practical schemes of TDDFT for open systems (TDDFT-OS) have been proposed by various authors.[5,7–17]

TDDFT-OS methods have been applied to study time-dependent electron transport through nanoelectronic devices, in which electron conductors of nanoscopic sizes are connected to macroscopic electrodes. Recently, by extending the applicability of TDDFT-OS, Wang *et al.* have simulated the transient electron dynamics on two-dimensional (2D) surface of a graphene monolayer[18] and electron transfer across the interface of a molecule-graphene composite. In these applications of TDDFT-OS, the nanodevice or the adsorbed molecule of primary interest is taken as an open system, while the surrounding bulk material or electron reservoir is treated as the environment.

In the framework of TDDFT-OS, the real-time dynamics of an open electronic system is characterized by a formally closed equation of motion (EOM) for the Kohn-Sham (KS) reduced single-electron density matrix of the open system.[5,17] The influence of the αth reservoir is completely accounted for through the reservoir spectral matrix $\mathbf{\Lambda}_\alpha(\epsilon)$, whose elements are defined by (hereafter, we use boldface to label matrices having the dimension of the open system)

$$\mathbf{\Lambda}_{\alpha,\mu\nu}(\epsilon) \equiv \pi \sum_{k\in\alpha} \delta(\epsilon - \epsilon_{\alpha k}) t^*_{\alpha k \mu} t_{\alpha k \nu}. \qquad (1)$$

Here, μ and ν represent the local basis functions that span the physical space of the open system, k denotes a KS orbital of isolated αth reservoir with the energy $\epsilon_{\alpha k}$, and $t_{\alpha k \mu}$ is the coupling strength between system orbital $|\mu\rangle$ and reservoir state $|k\rangle$. Obviously, the ϵ-dependent matrix $\mathbf{\Lambda}_\alpha(\epsilon)$ conveys the information about the intrinsic electronic structure of the αth reservoir.

For more efficient implementation of TDDFT-OS, a commonly used but somewhat crude approximation for $\mathbf{\Lambda}_\alpha(\epsilon)$ is the wide-band limit (WBL) approximation. With the WBL, the ϵ-dependence of $\mathbf{\Lambda}_\alpha(\epsilon)$ is neglected and a constant reservoir spectral matrix is used.[5,19–23] Consequently, the resulting numerical procedure is largely simplified. However, the WBL becomes less accurate when the electron dynamics is driven by external fields of large amplitudes or high frequencies.

a)xz58@ustc.edu.cn
b)yamcy@csrc.ac.cn

142, 144112-1

The complex absorbing potential (CAP) method has been developed to resolve the energy dependence of $\mathbf{\Lambda}_\alpha(\epsilon)$.[24–29] In this method, an absorbing potential is applied at the boundary of the open system, which provides the "driving force" for the exchange of electrons between αth reservoir and the open system. $\mathbf{\Lambda}_\alpha(\epsilon)$ or the absorbing potential is determined by computing the Green's function of the system plus a finite region of reservoir under a constraining potential. To accurately account for the effects of $\mathbf{\Lambda}_\alpha(\epsilon)$, usually a rather large region of reservoir needs to be included. This could make the subsequent TDDFT calculations somewhat time-consuming.

A formally exact TDDFT-OS has been established based on nonequilibrium Green's function (NEGF).[17] In the TDDFT-NEGF scheme, a set of linearly coupled EOM need to be solved, and each EOM corresponds to $\mathbf{\Lambda}_\alpha(\epsilon)$ at an energy point ϵ. This inevitably makes any practical calculation rather expensive, because usually the reservoir is comprised of bulk materials of complex band structures. Therefore, a large number of energy points N_ϵ (and equations) are required to ensure the accuracy of numerical outcomes. One way to reduce the computational cost is to introduce a set of basis functions to decompose $\mathbf{\Lambda}_\alpha(\epsilon)$. For instance, in our previous works,[17,18,30,31] we have used Lorentzian functions for the decomposition of $\mathbf{\Lambda}_\alpha(\epsilon)$,

$$\mathbf{\Lambda}_\alpha(\epsilon) \simeq \hat{\mathbf{\Lambda}}_\alpha(\epsilon) = \sum_{d=1}^{N_d} \frac{1}{(\epsilon - \Omega_d)^2 + W_d^2} \bar{\mathbf{\Lambda}}_{\alpha d}. \qquad (2)$$

Here, Ω_d (W_d) is the center (width) of dth Lorentzian basis function and $\bar{\mathbf{\Lambda}}_{\alpha d}$ is the corresponding coefficient matrix. The values of $\{\Omega_d, W_d, \bar{\mathbf{\Lambda}}_{\alpha d}\}$ are determined through a least-square fit to the exact $\mathbf{\Lambda}_\alpha(\epsilon)$. An alternative TDDFT-NEGF can therefore be constructed, with each Lorentzian function corresponding to an EOM. An advantage of such a construction is that, to achieve the same level of accuracy, the number of Lorentzian functions required is much smaller than that of energy points, i.e., $N_d \ll N_\epsilon$. Therefore, the Lorentzian decomposition of Eq. (2) significantly reduces the number of EOM to solve and thus greatly saves the computational cost of TDDFT-OS.

It is important to note that by definition, $\mathbf{\Lambda}_\alpha(\epsilon)$ of Eq. (1) should be positive semi-definite at any energy ϵ. This is because the reservoir spectral function is proportional to the square of system-reservoir coupling multiplied by the reservoir surface density of states. Physically, each non-negative eigenvalue of $\mathbf{\Lambda}_\alpha(\epsilon)$ is associated with a characteristic time of electron relaxation from system to αth reservoir. Numerically, the positive semi-definiteness of $\mathbf{\Lambda}_\alpha(\epsilon)$ ensures all the EOMs are well-behaved in the long-time limit. However, with the Lorentzian decomposition of Eq. (2), the positive semi-definiteness is not guaranteed for the fitted spectral matrix $\hat{\mathbf{\Lambda}}_\alpha(\epsilon)$. As shown later in this paper, this could lead to the unphysical divergence in the time evolution of TDDFT-NEGF. Therefore, it is desirable to develop a new decomposition scheme which preserves the positive semi-definiteness of $\mathbf{\Lambda}_\alpha(\epsilon)$.

In this work, we will (1) develop a squared-Lorentzian decomposition scheme for $\mathbf{\Lambda}_\alpha(\epsilon)$, which preserves the semi-definiteness, (2) establish the practical TDDFT-OS formalism by utilizing the positivity-preserving spectral decomposition

scheme, and (3) demonstrate the numerical validity and practicality of the novel scheme through several examples.

The remainder of this paper is organized as follows. In Sec. II, we introduce the positivity-preserving squared-Lorentzian reservoir spectral decomposition scheme and derive the corresponding TDDFT-OS formalism. In Sec. III, the new method is applied to simulate the electron transport through a quasi-one-dimensional (quasi-1D) atomic chain, and the dynamics of an excess electron on a 2D graphene bilayer. We finally conclude this work in Sec. IV.

II. METHODOLOGY

A. TDDFT-EOM for an open system

For the sake of completeness and ease of presentation, we first give a brief summary of the TDDFT-OS formalism, and the detailed derivations and important aspects of the TDDFT-OS can be found in Refs. 5, 17, and 18. The basic equation is the EOM for the KS reduced single-electron density matrix as follows:

$$i\dot{\boldsymbol{\sigma}}(t) = [\boldsymbol{h}(t), \boldsymbol{\sigma}(t)] - i \sum_\alpha \boldsymbol{Q}_\alpha(t). \qquad (3)$$

Here, $\boldsymbol{h}(t)$ is the KS Hamiltonian matrix for the open system, $\boldsymbol{\sigma}(t)$ denotes the reduced single-electron density matrix, and $\boldsymbol{Q}_\alpha(t)$ is the dissipation term. The $\boldsymbol{Q}_\alpha(t)$ term captures all the dissipative processes between the α-reservoir and the open system, including energy dissipation, electron transfer, and phase relaxation.

The dissipation term $\boldsymbol{Q}_\alpha(t)$ can be expressed by NEGF as follows:[17]

$$\boldsymbol{Q}_\alpha(t) = -i\,[\boldsymbol{\varphi}_\alpha(t) - \boldsymbol{\varphi}_\alpha^\dagger(t)], \qquad (4)$$

$$\boldsymbol{\varphi}_\alpha(t) = i \int_{-\infty}^t d\tau [\boldsymbol{G}^<(t,\tau)\boldsymbol{\Sigma}_\alpha^>(\tau,t) - \boldsymbol{G}^>(t,\tau)\boldsymbol{\Sigma}_\alpha^<(\tau,t)]. \qquad (5)$$

Here, $\boldsymbol{G}^<(t,\tau)$ and $\boldsymbol{G}^>(t,\tau)$ are the lesser and greater Green's functions of the open system, and $\boldsymbol{\Sigma}_\alpha^<(\tau,t)$ and $\boldsymbol{\Sigma}_\alpha^>(\tau,t)$ denote the lesser and greater self-energies due to the coupling to the α-reservoir, respectively. Note that all the matrices involved in Eqs. (3)–(5) have the same dimension corresponding to the Hilbert space of the open system. The lesser self-energy is associated with the reservoir spectral matrix $\mathbf{\Lambda}_\alpha(\epsilon)$ via

$$\boldsymbol{\Sigma}_\alpha^<(t,\tau) = e^{-i\int_\tau^t d\bar{t}\,\Delta_\alpha(\bar{t})} \widetilde{\boldsymbol{\Sigma}}_\alpha^<(t-\tau)$$
$$= \frac{i}{\pi} e^{-i\int_\tau^t d\bar{t}\,\Delta_\alpha(\bar{t})} \int d\epsilon\, \mathbf{\Lambda}_\alpha(\epsilon) f_\alpha(\epsilon)\, e^{-i\epsilon(t-\tau)}. \qquad (6)$$

Here, $\Delta_\alpha(t)$ is the time-dependent change of chemical potential of α-reservoir, $\widetilde{\boldsymbol{\Sigma}}_\alpha^<(t-\tau)$ is the equilibrium-state self-energy which assumes the translational invariance in time, and $f_\alpha(\epsilon) \equiv 1/[e^{\beta(\epsilon-\mu_\alpha)} + 1]$ is the Fermi function with $\beta = 1/k_B T$ and μ_α being the equilibrium chemical potential of α-reservoir.

Similarly, the greater self-energy $\Sigma_\alpha^>(t,\tau)$ is expressed by

$$
\begin{aligned}
\boldsymbol{\Sigma}_\alpha^>(t,\tau) &= e^{-i\int_\tau^t d\bar{t}\,\Delta_\alpha(\bar{t})}\,\widetilde{\boldsymbol{\Sigma}}_\alpha^>(t-\tau) \\
&= -\frac{i}{\pi}\,e^{-i\int_\tau^t d\bar{t}\,\Delta_\alpha(\bar{t})} \\
&\quad \times \int d\epsilon\,\boldsymbol{\Lambda}_\alpha(\epsilon)[1-f_\alpha(\epsilon)]\,e^{-i\epsilon(t-\tau)}.
\end{aligned}
\tag{7}
$$

Apparently, numerical solution of EOM (3) can be very expensive, since the evaluation of dissipation term $\boldsymbol{Q}_\alpha(t)$ through Eqs. (4) and (5) involves the computation of a rather complicated integral for each time t. A more efficient approach is desirable.

B. TDDFT-NEGF based on a Padé and Lorentzian decomposition (PLD) scheme

A formally rigorous and often more efficient TDDFT-OS formalism has been developed,[17] which is based on a combined PLD scheme for resolving the memory content of self-energies $\widetilde{\boldsymbol{\Sigma}}_\alpha^x(t)$ ($x =$ < or >).[17,30]

In the combined PLD scheme, $\boldsymbol{\Lambda}_\alpha(\epsilon)$ is expanded by Lorentzian functions, see Eq. (2), and the Fermi function $f_\alpha(\epsilon)$ is cast into a Padé form and then expanded as a sum of poles,[32]

$$
f_\alpha(\epsilon) \simeq \frac{1}{2} + \sum_{p=1}^{N_p} \frac{R_p}{\beta}\left(\frac{1}{\epsilon - \mu_\alpha - z_p^+/\beta} + \frac{1}{\epsilon - \mu_\alpha - z_p^-/\beta}\right).
\tag{8}
$$

Here, N_p is the number of Padé terms used, and $\{R_p\}$ and $\{z_p^\pm\}$ are the Padé coefficients and poles determined systematically through a diagonalization operation.[32] By inserting Eqs. (2) and (8) into Eqs. (6) and (7), we have the following exponential expansion for the equilibrium self-energies:[17,18,30]

$$
\widetilde{\boldsymbol{\Sigma}}_\alpha^x(t) \simeq
\begin{cases}
\displaystyle\sum_{k=1}^{N_k} \boldsymbol{C}_{\alpha k}^{x+}\, e^{-i\beta_{\alpha k}^+ t}, & (t < 0) \\[2ex]
\displaystyle\sum_{k=1}^{N_k} \boldsymbol{C}_{\alpha k}^{x-}\, e^{-i\beta_{\alpha k}^- t}, & (t > 0)
\end{cases},
\tag{9}
$$

where $N_k = N_d + N_p$, and $\{\boldsymbol{C}_{\alpha k}^{x\pm}\}$ and $\{\beta_{\alpha k}^\pm\}$ are the coefficient matrices and exponents, respectively.

With the exponential expansion of Eq. (9), $\boldsymbol{\varphi}_\alpha(t) = \sum_{k=1}^{N_k} \boldsymbol{\varphi}_{\alpha k}(t)$, and hence the EOM for $\boldsymbol{\sigma}(t)$ becomes

$$
i\dot{\boldsymbol{\sigma}}(t) = [\boldsymbol{h}(t), \boldsymbol{\sigma}(t)] - \sum_\alpha \sum_{k=1}^{N_k} [\boldsymbol{\varphi}_{\alpha k}(t) - \boldsymbol{\varphi}_{\alpha k}^\dagger(t)].
\tag{10}
$$

The auxiliary density matrices $\{\boldsymbol{\varphi}_{\alpha k}(t)\}$ satisfy the following EOM:

$$
\begin{aligned}
i\dot{\boldsymbol{\varphi}}_{\alpha k}(t) &= [\boldsymbol{h}(t) - \Delta_\alpha(t) - \beta_{\alpha k}^+]\,\boldsymbol{\varphi}_{\alpha k}(t) \\
&\quad - i\,[\bar{\boldsymbol{\sigma}}(t)\boldsymbol{C}_{\alpha k}^{<+} + \boldsymbol{\sigma}(t)\boldsymbol{C}_{\alpha k}^{>+}] \\
&\quad + \sum_{\alpha'}\sum_{k'=1}^{N_k} \boldsymbol{\varphi}_{\alpha' k', \alpha k}(t),
\end{aligned}
\tag{11}
$$

$$
\begin{aligned}
i\dot{\boldsymbol{\varphi}}_{\alpha' k', \alpha k}(t) &= [-\Delta_\alpha(t) - \beta_{\alpha k}^+ + \Delta_{\alpha'}(t) + \beta_{\alpha' k'}^-] \\
&\quad \times \boldsymbol{\varphi}_{\alpha' k', \alpha k}(t) - i\boldsymbol{\varphi}_{\alpha' k'}^\dagger(t)[\boldsymbol{C}_{\alpha k}^{>+} - \boldsymbol{C}_{\alpha k}^{<+}] \\
&\quad + i\,[\boldsymbol{C}_{\alpha' k'}^{>-} - \boldsymbol{C}_{\alpha' k'}^{<-}]\,\boldsymbol{\varphi}_{\alpha k}(t),
\end{aligned}
\tag{12}
$$

where $\bar{\boldsymbol{\sigma}}(t) = \boldsymbol{I} - \boldsymbol{\sigma}(t)$ with $\boldsymbol{I}$ being the identity matrix. Equations (10)–(12) thus constitute a set of EOM for $\{\boldsymbol{\sigma}(t), \boldsymbol{\varphi}_{\alpha k}(t),$ $\boldsymbol{\varphi}_{\alpha' k', \alpha k}(t)\}$ through NEGF scheme, and the EOMs are self-closed. The total number of basic variables is $N_k^2 + N_k + 1$.

The above TDDFT-NEGF constructed based on the PLD scheme has been applied successfully to simulate the real-time electronic dynamics in 1D and 2D open systems. However, as already discussed in Sec. I, the PLD scheme does not guarantee preserving the positive semi-definiteness of $\boldsymbol{\Lambda}_\alpha(\epsilon)$. Consequently, Eqs. (10)–(12) may be rather unstable, and occasionally they even lead to unphysical divergence in the long-time limit. Numerical example will be given in Sec. III.

C. TDDFT-NEGF based on a Padé and squared-Lorentzian decomposition (PSLD) scheme

To preserve the positive semi-definiteness of $\boldsymbol{\Lambda}_\alpha(\epsilon)$, we propose to replace the Lorentzian expansion of Eq. (2) by the following decomposition:

$$
\boldsymbol{\Lambda}_\alpha(\epsilon) \simeq \hat{\boldsymbol{\Lambda}}_\alpha(\epsilon) = \boldsymbol{L}_\alpha^t(\epsilon)\boldsymbol{L}_\alpha(\epsilon),
\tag{13}
$$

$$
\boldsymbol{L}_\alpha(\epsilon) = \sum_{d=1}^{N_d} \frac{1}{(\epsilon - \Omega_d)^2 + W_d^2}\,\bar{\boldsymbol{L}}_{\alpha d}.
\tag{14}
$$

In Eq. (13), $\boldsymbol{L}_\alpha^t(\epsilon)$ denotes the transpose of the auxiliary matrix $\boldsymbol{L}_\alpha(\epsilon)$. It is $\boldsymbol{L}_\alpha(\epsilon)$ rather than $\hat{\boldsymbol{\Lambda}}_\alpha(\epsilon)$ that is expanded by Lorentzian basis functions, with Ω_d (W_d) being the center (width) of dth Lorentzian function and $\bar{\boldsymbol{L}}_{\alpha d}$ the corresponding coefficient matrix.

Obviously, the square form of Eq. (13) ensures that all eigenvalues of the fitted reservoir spectral matrix $\hat{\boldsymbol{\Lambda}}_\alpha(\epsilon)$ are non-negative at any ϵ. Therefore, Eqs. (8), (13), and (14) constitute a combined PSLD scheme, with which the equilibrium self-energies $\widetilde{\boldsymbol{\Sigma}}_\alpha^x(t)$ are expanded as follows:

$$
\widetilde{\boldsymbol{\Sigma}}_\alpha^x(t) \simeq
\begin{cases}
\displaystyle\sum_{k=1}^{N_k} \boldsymbol{A}_{\alpha k}^{x+}\, e^{-i\gamma_{\alpha k}^+ t} + \sum_{d=1}^{N_d} \boldsymbol{B}_{\alpha d}^{x+}\, t\, e^{-i\gamma_{\alpha d}^+ t}, & (t < 0) \\[2ex]
\displaystyle\sum_{k=1}^{N_k} \boldsymbol{A}_{\alpha k}^{x-}\, e^{-i\gamma_{\alpha k}^- t} + \sum_{d=1}^{N_d} \boldsymbol{B}_{\alpha d}^{x-}\, t\, e^{-i\gamma_{\alpha d}^- t}, & (t > 0)
\end{cases},
\tag{15}
$$

where $N_k = N_d + N_p$. The detailed expressions for the coefficient matrices $\{\boldsymbol{A}_{\alpha k}^{x\pm}, \boldsymbol{B}_{\alpha d}^{x\pm}\}$ and the exponents $\{\gamma_{\alpha d}^\pm\}$ are given in Appendix A.

Equation (15) is distinctly different from Eq. (9). Unlike the PLD scheme which leads to a pure exponential expansion of $\widetilde{\boldsymbol{\Sigma}}_\alpha^x(t)$, the PSLD scheme gives rise to additional polynomial exponential memory components that are proportional to $t\,e^{-i\gamma_{\alpha d}^\pm t}$. These new components originate from the second-order poles of $\hat{\boldsymbol{\Lambda}}_\alpha(\epsilon)$ given by Eq. (13). Note that the time derivative of a polynomial exponential function $t^n e^{\gamma t}$ only involves polynomial exponentials of lower orders. Therefore, a set of formally closed EOM can be constructed based on Eq. (15). In fact, the polynomial exponential type of reservoir memory function has been adopted to construct a hierarchical set of quantum dynamics equations for studying the dissipative dynamics of a spin-boson model.[33]

We first define the following three types of first-tier auxiliary density matrices:

$$\boldsymbol{\varphi}_{\alpha k}^{a}(t) = i \int_{-\infty}^{t} d\tau \, \boldsymbol{G}^{<}(t,\tau) \, \boldsymbol{E}_{\alpha k}^{+}(\tau,t), \qquad (16)$$

$$\boldsymbol{\varphi}_{\alpha k}^{b}(t) = -i \int_{-\infty}^{t} d\tau \, \boldsymbol{G}^{>}(t,\tau) \, \boldsymbol{E}_{\alpha k}^{+}(\tau,t), \qquad (17)$$

$$\boldsymbol{\varphi}_{\alpha d}^{c}(t) = i \int_{-\infty}^{t} d\tau \, \big[\boldsymbol{G}^{<}(t,\tau) \boldsymbol{\Upsilon}_{\alpha d}^{>}(\tau,t) \\ - \boldsymbol{G}^{>}(t,\tau) \boldsymbol{\Upsilon}_{\alpha d}^{<}(\tau,t) \big]. \qquad (18)$$

Here, k and d label the exponential and polynomial exponential components on the right-hand side of Eq. (15), respectively; and $E_{\alpha k}^{\sigma}(\tau,t)$ ($\sigma = +$ or $-$) and $\boldsymbol{\Upsilon}_{\alpha d}^{x}(\tau,t)$ ($x = >$ or $<$) are defined as follows:

$$E_{\alpha k}^{\sigma}(\tau,t) = e^{-\sigma i\left[\gamma_{\alpha k}^{\sigma}(\tau-t) + \int_{t}^{\tau} d\bar{t} \, \Delta_{\alpha}(\bar{t})\right]}, \qquad (19)$$

$$\boldsymbol{\Upsilon}_{\alpha d}^{x}(\tau,t) = \boldsymbol{B}_{\alpha d}^{x+}(\tau-t) \, e^{-i\left[\gamma_{\alpha d}^{+}(\tau-t) + \int_{t}^{\tau} d\bar{t} \, \Delta_{\alpha}(\bar{t})\right]}. \qquad (20)$$

By comparing Eqs. (16)–(18) and Eqs. (3)–(5), the following EOM for $\boldsymbol{\sigma}(t)$ is obtained readily:

$$i\dot{\boldsymbol{\sigma}}(t) = [\boldsymbol{h}(t), \boldsymbol{\sigma}(t)] - \sum_{\alpha}\sum_{d=1}^{N_d}[\boldsymbol{\varphi}_{\alpha d}^{c}(t) - \boldsymbol{\varphi}_{\alpha d}^{c\dagger}(t)]$$

$$- \sum_{\alpha}\sum_{k=1}^{N_k}\big[\boldsymbol{\varphi}_{\alpha k}^{a}(t)\boldsymbol{A}_{\alpha k}^{>+} + \boldsymbol{\varphi}_{\alpha k}^{b}(t)\boldsymbol{A}_{\alpha k}^{<+} - \text{h.c.}\big]. \qquad (21)$$

The EOMs for the first-tier auxiliary density matrices $\{\boldsymbol{\varphi}_{\alpha k}^{a}(t), \boldsymbol{\varphi}_{\alpha k}^{b}(t), \boldsymbol{\varphi}_{\alpha d}^{c}(t)\}$ are as follows:

$$i\dot{\boldsymbol{\varphi}}_{\alpha k}^{a}(t) = -i\boldsymbol{\sigma}(t) + \big[\boldsymbol{h}(t) - \gamma_{\alpha k}^{+} - \Delta_{\alpha}(t)\big]\boldsymbol{\varphi}_{\alpha k}^{a}(t)$$

$$+ \sum_{\alpha'}\sum_{d=1}^{N_d}\boldsymbol{\varphi}_{\alpha'd,\alpha k}^{ca}(t) + \sum_{\alpha'}\sum_{k'=1}^{N_k}\boldsymbol{A}_{\alpha'k'}^{>-}\boldsymbol{\varphi}_{\alpha'k',\alpha k}^{ba}(t)$$

$$+ \sum_{\alpha'}\sum_{k'=1}^{N_k}\boldsymbol{A}_{\alpha'k'}^{<-}\boldsymbol{\varphi}_{\alpha'k',\alpha k}^{aa}(t), \qquad (22)$$

$$i\dot{\boldsymbol{\varphi}}_{\alpha k}^{b}(t) = -i[\boldsymbol{I} - \boldsymbol{\sigma}(t)] + \sum_{\alpha'}\sum_{k'=1}^{N_k}\boldsymbol{A}_{\alpha'k'}^{<-}\boldsymbol{\varphi}_{\alpha'k',\alpha k}^{ab}(t)$$

$$+ \big[\boldsymbol{h}(t) - \gamma_{\alpha k}^{+} - \Delta_{\alpha}(t)\big]\boldsymbol{\varphi}_{\alpha k}^{b}(t)$$

$$+ \sum_{\alpha'}\sum_{k'=1}^{N_k}\boldsymbol{A}_{\alpha'k'}^{>-}\boldsymbol{\varphi}_{\alpha'k',\alpha k}^{bb}(t) + \sum_{\alpha'}\sum_{d=1}^{N_d}\boldsymbol{\varphi}_{\alpha'd,\alpha k}^{cb}(t), \qquad (23)$$

$$i\dot{\boldsymbol{\varphi}}_{\alpha d}^{c}(t) = \big[\boldsymbol{h}(t) - \gamma_{\alpha d}^{+} - \Delta_{\alpha}(t)\big]\boldsymbol{\varphi}_{\alpha d}^{c}(t)$$

$$- i\big[\boldsymbol{\varphi}_{\alpha d}^{a}(t)\boldsymbol{B}_{\alpha d}^{>+} + \boldsymbol{\varphi}_{\alpha d}^{b}(t)\boldsymbol{B}_{\alpha d}^{<+}\big]$$

$$+ \sum_{\alpha'}\sum_{k=1}^{N_k}\big[\boldsymbol{A}_{\alpha'k}^{<-}\boldsymbol{\varphi}_{\alpha'k,\alpha d}^{ac}(t) + \boldsymbol{A}_{\alpha'k}^{>-}\boldsymbol{\varphi}_{\alpha'k,\alpha d}^{bc}(t)\big]$$

$$+ \sum_{\alpha'}\sum_{d'=1}^{N_d}\boldsymbol{\varphi}_{\alpha'd',\alpha d}^{cc}(t). \qquad (24)$$

Here, $\{\boldsymbol{\varphi}_{\alpha'm',\alpha m}^{ij}(t)\}$ ($i,j = a,b,c$ and $m = k,d$) are the second-tier auxiliary density matrices, whose definitions and EOM are presented in Appendix B. Note that the time derivatives of $\{\boldsymbol{\varphi}_{\alpha'm'\alpha m}^{ij}(t)\}$ involve only the first- and second-tier auxiliary density matrices. Consequently, the EOMs for $\{\boldsymbol{\sigma}(t), \boldsymbol{\varphi}_{\alpha m}^{i}(t),$

$\boldsymbol{\varphi}_{\alpha'm',\alpha m}^{ij}(t)\}$ form a set of closed equations, and the total number of basic variables is $M^2 + M + 1$ with $M = 2N_k + N_d$. Therefore, for the same system, the TDDFT-NEGF constructed based on the PSLD scheme requires about nine times of memory as that of the PLD counterpart.

As will be demonstrated in Sec. III, the new TDDFT-NEGF established with the squared-Lorentzian decomposition of $\boldsymbol{\Lambda}_{\alpha}(\epsilon)$ is quantitatively accurate and numerically much more stable than the EOM constructed by using the PLD scheme.

III. NUMERICAL RESULTS AND DISCUSSIONS

To demonstrate its validity and usefulness, the PSLD scheme and its resulting TDDFT-NEGF approach as described in Sec. II C are applied to two types of systems: (1) quasi-1D atomic chains and (2) 2D bilayer graphene.

A. Application of PSLD scheme based TDDFT-NEGF approach to quasi-1D atomic chains

Figure 1 depicts an infinite long quasi-1D atomic chain with a width of n atoms. Within the framework of TDDFT-OS, the atoms in the green region constitute the (open) system, while all other atoms are taken as the surrounding environment. Such a model system represents a prototypical nano-electronic device. We adopt a nearest-neighbor tight-binding model Hamiltonian to describe the atomic chain: the on-site energies are set to zero, and the coupling between any two nearest-neighboring atoms is set to $\gamma = 1.0$ eV.

We first examine the projected density of states (PDOSs) of the system (the green region in Fig. 1) at equilibrium. The PDOS $N(\epsilon)$ is computed by

$$N(\epsilon) = -\frac{1}{\pi}\,\text{Im}\left\{\text{tr}\big[\epsilon\boldsymbol{I} - \boldsymbol{h} - \widetilde{\boldsymbol{\Sigma}}^{r}(\epsilon)\big]^{-1}\right\}. \qquad (25)$$

Here, $\widetilde{\boldsymbol{\Sigma}}^{r}(\epsilon) = \sum_{\alpha}\widetilde{\boldsymbol{\Sigma}}_{\alpha}^{r}(\epsilon) = \boldsymbol{\Gamma}(\epsilon) - i\boldsymbol{\Lambda}(\epsilon)$ is the equilibrium retarded self-energy arising from the system-reservoir couplings, and $\boldsymbol{\Gamma}(\epsilon)$ is deduced from $\boldsymbol{\Lambda}(\epsilon) = \sum_{\alpha}\boldsymbol{\Lambda}_{\alpha}(\epsilon)$ via the Kramers-Kronig relation.[34] A renormalization approach[35] utilizing the translational symmetry along the chain axis is employed, which yields highly accurate $\widetilde{\boldsymbol{\Sigma}}_{\alpha}^{r}(\epsilon)$ and $\boldsymbol{\Lambda}_{\alpha}(\epsilon)$. Using the Lorentzian decomposition of Eq. (2) or the squared-Lorentzian decomposition of Eqs. (13) and (14), the fitted $\widehat{\boldsymbol{\Lambda}}_{\alpha}(\epsilon)$ and $\widetilde{\boldsymbol{\Sigma}}_{\alpha}^{r}(\epsilon)$ are obtained, and then the corresponding PDOS of the system is evaluated through Eq. (25).

Figure 2(a) compares the PDOS of a quasi-1D atomic chain computed with $\widetilde{\boldsymbol{\Sigma}}_{\alpha}^{r}(\epsilon)$ obtained by Lorentzian or squared-Lorentzian decomposition for $\boldsymbol{\Lambda}_{\alpha}(\epsilon)$. For both decomposition
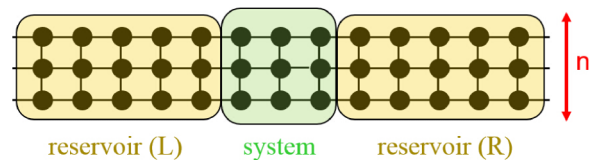

FIG. 1. Schematic diagram of a quasi-1D atomic chain with a finite width n. Within the framework of TDDFT-OS, the green region is taken as the (open) system, and the yellow regions are treated as electron reservoirs (the environment) for the system.
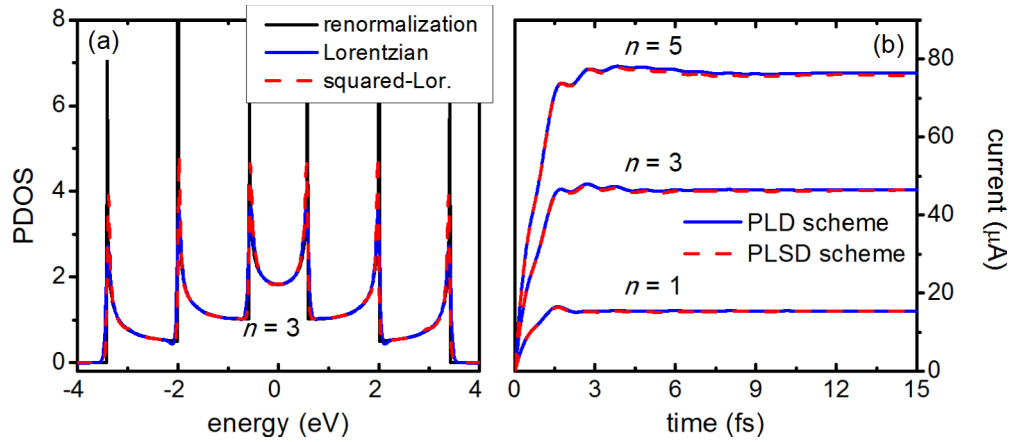
FIG. 2. (a) PDOS of an atomic chain of width $n = 3$ computed with $\Lambda_\alpha(\epsilon)$ evaluated by a renormalization approach[35] (black line) or approximated by the Lorentzian decomposition scheme (blue line) or the squared-Lorentzian decomposition scheme (red line). (b) Time-dependent currents through atomic chains of different widths ($n = 1, 3, 5$) in response to a switch-on voltage of amplitude $V_L = -V_R = 0.1$ V. The blue and red lines are obtained from the TDDFT-NEGF constructed based on the PLD and PSLD schemes, respectively.

schemes, 48 Lorentzian basis functions are used. The Lorentzian functions are centered at 16 equally spaced energy points, and each center is assigned with 3 different widths ($N_d = 48$).

As a benchmark, the PDOS obtained using the renormalization approach is also shown in Fig. 2(a). It is clearly seen that all the three PDOS curves agree well with each other, except the minor deviations at the energies of van Hove singularities. Such a quantitative agreement justifies the accuracy of the squared-Lorentzian decomposition of $\Lambda_\alpha(\epsilon)$.

We then investigate the time-dependent electron transport through atomic chains of different widths n, assuming a bias voltage is applied across the system region. The time-dependent response current flowing through the α-reservoir is calculated by[5]

$$I_\alpha(t) = -\mathrm{tr}[\boldsymbol{Q}_\alpha(t)], \qquad (26)$$

where $\boldsymbol{Q}_\alpha(t)$ is the dissipative term defined by Eq. (4). We employ the TDDFT-NEGF approaches presented, respectively, in Secs. II B and II C to study the transient electron dynamics driven by the voltage.

Initially, the atomic chain is in a thermal equilibrium state at the temperature $T = 100$ K. It is found that 20 Padé terms ($N_p = 20$) are sufficient to reproduce accurately the Fermi function through Eq. (8). A bias voltage is turned on antisymmetrically across the two leads ($\alpha = L$ and R) from the time $t_0 = 0$ and is then maintained at a constant amplitude of $V_L = -V_R = 0.1$ V. The fourth-order Runge-Kutta algorithm[36] is adopted to propagate the EOM in time. The time-dependent response currents calculated with the TDDFT-NEGF constructed based on both the PLD and PSLD schemes are shown in Fig. 2(b) for chains of widths $n = 1, 3, 5$. The two sets of data agree remarkably well with each other for all the three chains studied.

Note that in the long-time limit ($t \to \infty$), the system approaches asymptotically to a steady state. The steady currents, $I(\infty) = |I_\alpha(t \to \infty)|$, for the three chains ($n = 1, 3, 5$) are 15.49 μA, 46.47 μA, and 76.66 μA, respectively. The values of steady currents conform well to the relation $I(\infty) = n g_0 (V_L - V_R)$, with $g_0 = 2e^2/h$ being the conductance quantum. This reflects the fact that the chain of width n possesses exactly $2n$

conduction channels (considering spin degeneracy) for electron transport along the axial direction.

The above simulations on quasi-1D chains clearly demonstrate that both the PLD and PSLD schemes accurately resolve the memory contents of reservoirs and hence reliably account for their influences on the electronic dynamics of open systems, as long as the resulting EOMs remain numerically stable.

B. Application of PSLD scheme based TDDFT-NEGF approach to 2D bilayer graphene

We now turn to a more complex (and hence more challenging) system—a Bernal (A-B) stacked graphene bilayer—as sketched in Fig. 3(a). A homogeneous electric field is applied perpendicular to the graphene planes, which is known to open a finite gap in the band structure of bilayer graphene.[37] We adopt a nearest-neighbor tight-binding model Hamiltonian to describe the p_z orbitals of all carbon atoms,[38]

$$\begin{aligned}
H_T = &\sum_{i=1}^{2} \varepsilon_i \left(a_{i,m}^\dagger a_{i,m} + b_{i,m}^\dagger b_{i,m} \right) \\
&- t_{//} \sum_{i=1}^{2} \sum_{m,n_m} \left(a_{i,m}^\dagger b_{i,n_m} + b_{i,n_m}^\dagger a_{i,m} \right) \\
&- t_\perp \sum_m \left(a_{1,m}^\dagger b_{2,m} + b_{2,m}^\dagger a_{1,m} \right).
\end{aligned} \qquad (27)$$

Here, $i = 1, 2$ labels the top or bottom layer, $a_{i,m}^\dagger$ ($b_{i,m}$) creates (annihilates) an electron on mth atom of sublattice A (B) on ith layer, and n_m denotes the nearest neighbors of m. Due to the electron polarization in response to the applied electric field, the two graphene layers have different potential energies. To account for the effect of electric field, the on-site energies in Eq. (27) are set as $\varepsilon_1 = -\varepsilon_2 = -0.1$ eV. The second and third terms on the right-hand side of Eq. (27) describe the intra- and inter-layer couplings, respectively, and the coupling strengths are set as $t_{//} = 2.7$ eV and $t_\perp = 0.2 \, t_{//}$. To demonstrate more obvious electron transfer between top layer and bottom layer, a larger inter-layer coupling strength
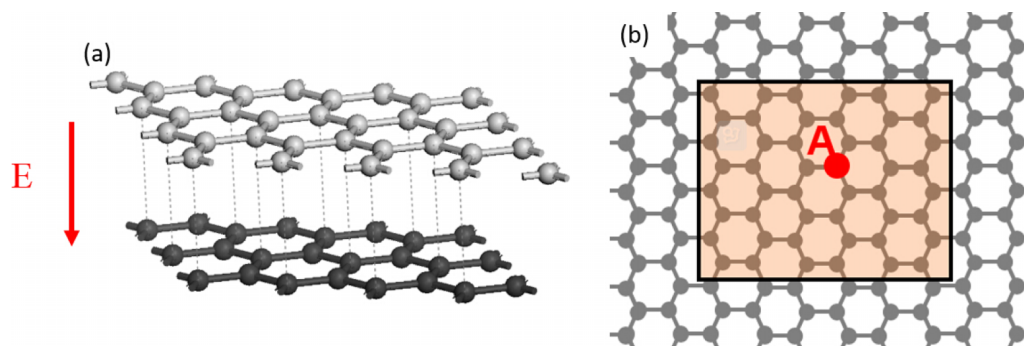
FIG. 3. (a) Side view of the bilayer graphene under study. The atoms in light and dark gray belong to the top and bottom layers, respectively. The dashed lines indicate nonzero couplings between neighboring atoms of different layers. An electric field is applied perpendicular to the graphene planes. (b) Top view of the bilayer graphene. The shaded rectangular region is treated as the open system, which includes 48 carbon atoms in each layer. The rest atoms constitute the environment or electron reservoir.

$(t_\perp = 0.54$ eV$)$ is used, compared against strengths at optimal inter-layer distance.[37,39,40]

To apply the TDDFT-OS, the bilayer graphene is partitioned into two parts: the open system and its environment. The system is represented by the shaded region in Fig. 3(b), which consists of 48 atoms in each layer. Because of the 2D structure of graphene, a k-sampling scheme is employed to compute the reservoir spectral matrix.[41] Similarly as in Sec. III A, $\Lambda_\alpha(\epsilon)$ are also approximated by the Lorentzian and squared-Lorentzian decompositions. For both schemes, we set 15 equally spaced energy points between -8.1 and 8.1 eV, and each center is assigned with 3 different widths. In addition, to capture the small band gap near the Fermi energy opened by the electric field, a very narrow Lorentzian of width 0.05 eV is also invoked. Therefore, in total, $N_d = 46$ Lorentzian basis functions are used.

Figure 4(a) plots the PDOS of system obtained via Eq. (25) with $\Lambda_\alpha(\epsilon)$ computed with the three different schemes. Apparently, the three curves agree reasonably well with each other. This thus verifies that the squared-Lorentzian decomposition

can accurately reproduce the electronic structure of the open system.

We then investigate the real-time electron dynamics on the bilayer graphene. Initially, the whole system is in thermal equilibrium state at temperature $T = 300$ K. At a certain time (say, at $t_0 = 0$), an excess electron is injected onto atom A of the top layer (see Fig. 3(b)). The excess electron represents injection of electrons from dye molecules to TiO_2 surface in dye-sensitized solar cells or excited electron resulted from oxidation of water in biomimetic water-splitting complex. This results in an instantaneous change in the reduced single-electron density matrix: $\sigma_{AA}(t_0^+) = \sigma_{AA}^{eq} + 1$, with σ_{AA}^{eq} being the equilibrium electron occupation number on atom A. At $t > t_0$, the excess electron moves along the graphene surface or transits between the top and bottom layers. Consequently, as time goes on, the distribution of excess electron is expected to smear out on both layers.

The time evolution of the excess electron is simulated by the TDDFT-NEGF constructed based on both PLD and PSLD schemes. In Fig. 4(b), we plot the variation of electron
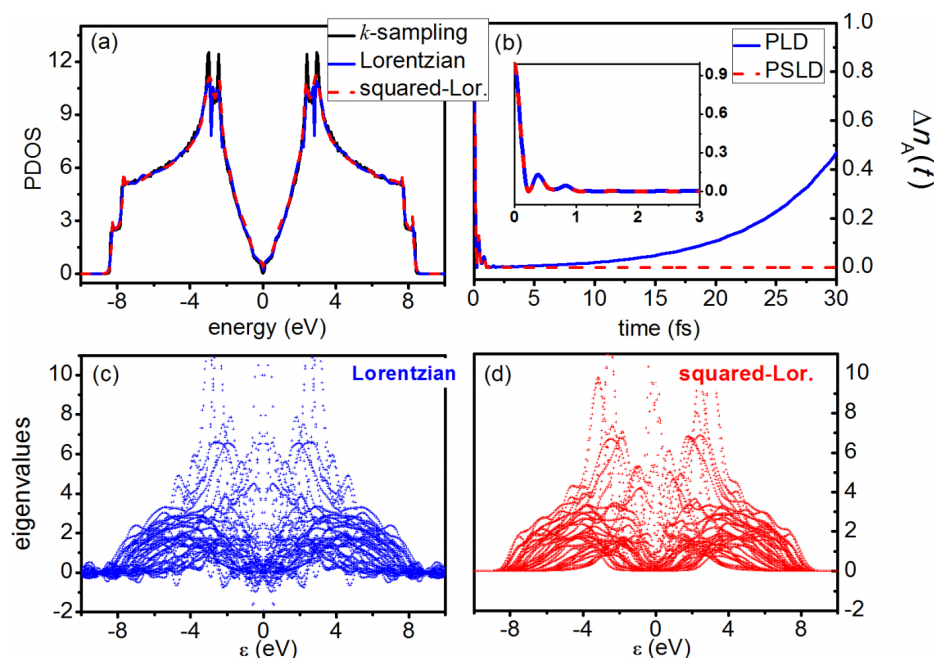

FIG. 4. (a) PDOS of the "system" part of bilayer graphene obtained by using the k-sampling scheme (black line), Lorentzian decomposition scheme (blue line), and squared-Lorentzian decomposition scheme (red line). (b) Number of excess electrons inside the system region versus time. The inset magnifies the data of the first 3 fs. (c) and (d) display all the eigenvalues of $\Lambda(\epsilon)$ approximated by the Lorentzian and squared-Lorentzian decomposition schemes, respectively.

occupation number on atom A versus time, $\Delta n_A(t) = \sigma_{AA}(t) - \sigma_{AA}^{eq}$. The two sets of data agree well with each other within the first few femtoseconds; see the inset of Fig. 4(b). However, the result of PLD scheme starts to diverge from about $t = 10$ fs, and the unphysical divergence becomes more severe at a longer time. In contrast, the result of PSLD scheme remains very stable, and the initial equilibrium is correctly retrieved in the long-time limit, i.e., $\Delta n_A(t \rightarrow \infty) = 0$. It is worth noting that the divergence remains with different inter-layer coupling strengths, and the results show that PSLD scheme indeed removes the numerical divergence problem and improves the longtime stability of our TDDFT-OS.

To understand the origin of difference between the PLD and PSLD results, in Figs. 4(c) and 4(d), we plot all the eigenvalues of $\Lambda(\epsilon)$ fitted by Lorentzian and squared-Lorentzian decomposition schemes, respectively. It is clear that, while the overall distributions of eigenvalues are much alike, there is a significant distinction between the two panels: in Fig. 4(c), a number of negative eigenvalues are observed, with the largest negative values residing around the Fermi energy; while in Fig. 4(d), all the eigenvalues are non-negative. Therefore, the squared-Lorentzian decomposition scheme of Eqs. (13) and (14) indeed preserves the positive semi-definiteness of reservoir spectral matrix, which guarantees the numerical stability and convergence of the resulting TDDFT-NEGF approach.

It is interesting to examine the rate of electron dissipation from the system region to the surrounding bulk environment. To this end, we compute the number of excess electron inside the system region on ith layer, $\Delta N_i(t) = \sum_{m \in i} \sigma_{mm}(t) - \sigma_{mm}^{eq}$, with the PSLD based TDDFT-NEGF approach. Figures 5(a) and 5(b) depict $\Delta N_i(t)$ for the top ($i = 1$) and bottom ($i = 2$) layers, respectively. It is observed that the excess electron dissipates quickly to the environment on the top layer. The corresponding time scale is as short as 3 fs. Moreover, a fractional amount of electron is found to "leak" to the bottom layer through the inter-layer coupling $t_\perp$. This leads to a temporary maximum of electron number on the bottom layer at about 0.8 fs, which is followed by transient electron fluctuation and dissipation. As indicated by Fig. 5(b), it takes a relatively longer time (more than 12 fs) to restore the initial equilibrium for the bottom layer. Due to back and forth electron transfer between top layer and bottom layer, we can see a recurrence of electron in the bottom layer at around 9 fs. It is worth mentioning that the $\Delta N_i(t)$ obtained by the PLD based TDDFT-NEGF exhibit unphysical divergence within 2 fs (data not shown).
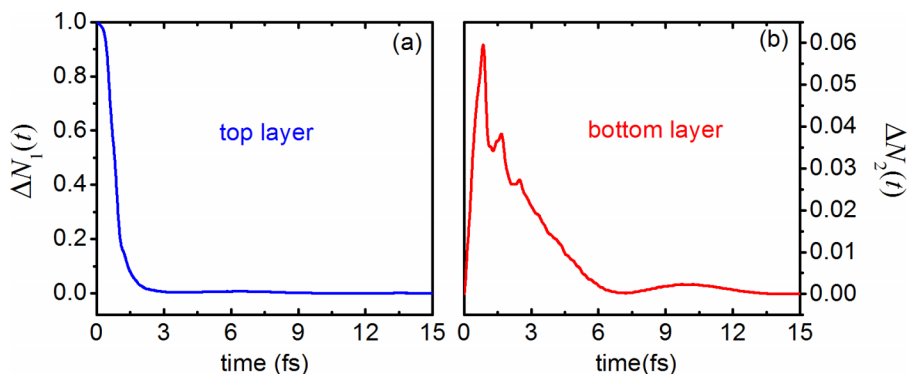
IV. CONCLUDING REMARKS

To conclude, in this work, we develop a novel scheme—the squared-Lorentzian decomposition scheme—for resolving the memory content and energetic structure of reservoir environment. By construction, the novel scheme has the advantage of preserving the positive semi-definiteness of reservoir spectral matrices. We further establish the TDDFT-NEGF based on the combined Padé and squared-Lorentzian decomposition scheme, which results in highly accurate and convergent electronic dynamics. The numerical divergence problem in previous PLD scheme is resolved and longtime stability is guaranteed. The validity and usefulness of our new approach are exemplified by simulations on quasi-1D atomic chains and 2D bilayer graphene systems. In particular, for the latter system, only the new approach is capable of yielding convergent dynamics in the long-time limit. The improved TDDFT-OS method thus provides a practical and reliable tool for theoretical investigation on time-dependent physical and chemical phenomena occurring at surfaces or interfaces of materials.

In this work, a simple tight-binding model is adopted to describe the system. Recently, a TDDFT-OS method formulated with non-orthogonal basis functions has been developed.[31] Utilizing the non-orthogonal basis formulation, the PSLD based TDDFT-NEGF approach may be implemented in conjunction with DFT or density-functional tight-binding methods to study realistic systems at first-principles level for applications in nanoelectronics, catalysis, and photovoltaics.[23,42-45]

APPENDIX A: DERIVATION OF Eq. (15)

The equilibrium self-energies are related to the reservoir spectral matrix $\Lambda_\alpha(\epsilon)$ via

$$\widetilde{\Sigma}_\alpha^<(t) = \frac{i}{\pi} \int d\epsilon \, \Lambda_\alpha(\epsilon) f_\alpha(\epsilon) \, e^{-i\epsilon t}, \tag{A1}$$

$$\widetilde{\Sigma}_\alpha^>(t) = -\frac{i}{\pi} \int d\epsilon \, \Lambda_\alpha(\epsilon)[1 - f_\alpha(\epsilon)] \, e^{-i\epsilon t}. \tag{A2}$$

FIG. 5. Time-varying number of excess electron inside the system region $\Delta N_i(t)$ on the (a) top ($i = 1$) and (b) bottom ($i = 2$) graphene layer.

With the squared-Lorentzian decomposition of Eqs. (13) and (14), $\Lambda_\alpha(\epsilon)$ is expanded by

$$
\Lambda_\alpha(\epsilon) \simeq \sum_{d=1}^{N_d} \sum_{d'=1}^{N_{d'}} \frac{1}{(\epsilon - \Omega_d)^2 + W_d^2}
$$
$$
\times \frac{1}{(\epsilon - \Omega_{d'})^2 + W_{d'}^2} \bar{L}_{\alpha d}^t \bar{L}_{\alpha d'}. \tag{A3}
$$

Using the complex contour integral technique along with the residue theorem, the expansion of Eq. (15) is achieved. The involving coefficient matrices and exponents are given as follows. The exponents $\{\gamma_{\alpha k}^\sigma\}$ ($\sigma = +$ or $-$) are

$$
\gamma_{\alpha k}^\sigma = \begin{cases} \Omega_k + \sigma i W_k, & 1 \leqslant k \leqslant N_d, \\ \mu_\alpha + z_k^\sigma/\beta, & N_d < k \leqslant N_d + N_p. \end{cases} \tag{A4}
$$

The coefficient matrices $\{A_{\alpha k}^{x\sigma}\}$ ($x = <$ or $>$) are

$$
A_{\alpha k}^{<\sigma} = \frac{i}{W_k} f_\alpha(\gamma_{\alpha k}^\sigma) Z_{\alpha k}^\sigma + \frac{-\sigma}{2W_k^2} P_{\alpha k}^\sigma \bar{L}_{\alpha k}^t \bar{L}_{\alpha k}
$$
$$
+ \frac{i}{2W_k^3} f_\alpha(\gamma_{\alpha k}^\sigma) \bar{L}_{\alpha k}^t \bar{L}_{\alpha k}, \tag{A5}
$$

$$
A_{\alpha k}^{>\sigma} = \frac{-i}{W_k} [1 - f_\alpha(\gamma_{\alpha k}^\sigma)] Z_{\alpha k}^\sigma + \frac{-\sigma}{2W_k^2} P_{\alpha k}^\sigma \bar{L}_{\alpha k}^t \bar{L}_{\alpha k}
$$
$$
+ \frac{-i}{2W_k^3} [1 - f_\alpha(\gamma_{\alpha k}^\sigma)] \bar{L}_{\alpha k}^t \bar{L}_{\alpha k} \tag{A6}
$$

for $1 \leqslant k \leqslant N_d$ and

$$
A_{\alpha k}^{<\sigma} = A_{\alpha k}^{>\sigma} = \frac{-\sigma 2 R_k}{\beta} \Lambda_\alpha(\gamma_{\alpha k}^\sigma) \tag{A7}
$$

for $N_d < k \leqslant N_d + N_p$. In Eq. (A5), $Z_{\alpha k}^\sigma$ and $P_{\alpha k}^\sigma$ are given by

$$
Z_{\alpha k}^\sigma = \sum_{d \neq k}^{N_d} \frac{1}{(\gamma_{\alpha k}^\sigma - \Omega_d)^2 + W_d^2} (\bar{L}_{\alpha k}^t \bar{L}_{\alpha d} + \bar{L}_{\alpha d}^t \bar{L}_{\alpha k}), \tag{A8}
$$

$$
P_{\alpha k}^\sigma = \sum_{p=1}^{N_p} \frac{R_p}{\beta} \left[\frac{1}{(\gamma_{\alpha k}^\sigma - \mu_\alpha - z_p^+/\beta)^2} + \frac{1}{(\gamma_{\alpha k}^\sigma - \mu_\alpha - z_p^-/\beta)^2} \right]. \tag{A9}
$$

The coefficient matrices $\{B_{\alpha d}^{x\sigma}\}$ are given by

$$
B_{\alpha d}^{<\sigma} = \frac{-\sigma i}{2W_d^2} f_\alpha(\gamma_{\alpha d}^\sigma) \bar{L}_{\alpha d}^t \bar{L}_{\alpha d}, \tag{A10}
$$

$$
B_{\alpha d}^{>\sigma} = \frac{\sigma i}{2W_d^2} [1 - f_\alpha(\gamma_{\alpha d}^\sigma)] \bar{L}_{\alpha d}^t \bar{L}_{\alpha d}. \tag{A11}
$$

APPENDIX B: SECOND-TIER AUXILIARY DENSITY MATRICES AND THEIR EOM IN THE COMBINED PADÉ AND SQUARED-LORENTZIAN DECOMPOSITION SCHEME

In the PSLD scheme, the nine types of second-tier auxiliary density matrices $\{\varphi_{\alpha'm',\alpha m}^{ij}(t)\}$ ($i, j = a, b, c$ and $m = k, d$) are defined as follows:

$$
\varphi_{\alpha'k',\alpha k}^{aa}(t) = i \int_{-\infty}^t d\tau \int_{-\infty}^{+\infty} d\bar{t} \left[-\vartheta(t - \bar{t}) E_{\alpha'k'}^-(t,\bar{t}) \mathbf{G}^<(\bar{t},\tau) + E_{\alpha'k'}^-(t,\bar{t}) \mathbf{G}^a(\bar{t},\tau) \right] E_{\alpha k}^+(\tau,t), \tag{B1}
$$

$$
\varphi_{\alpha'k',\alpha k}^{ba}(t) = i \int_{-\infty}^t d\tau \int_{-\infty}^{+\infty} d\bar{t} \, \vartheta(t - \bar{t}) \, E_{\alpha'k'}^-(t,\bar{t}) \mathbf{G}^<(\bar{t},\tau) E_{\alpha k}^+(\tau,t), \tag{B2}
$$

$$
\varphi_{\alpha'd,\alpha k}^{ca}(t) = i \int_{-\infty}^t d\tau \int_{-\infty}^{+\infty} d\bar{t} \left\{ -\vartheta(t - \bar{t}) \left[\Upsilon_{\alpha'd}^<(t,\bar{t}) - \Upsilon_{\alpha'd}^>(t,\bar{t}) \right] \mathbf{G}^<(\bar{t},\tau) + \Upsilon_{\alpha'k'}^<(t,\bar{t}) \mathbf{G}^a(\bar{t},\tau) \right\} E_{\alpha k}^+(\tau,t), \tag{B3}
$$

$$
\varphi_{\alpha'k',\alpha k}^{ab}(t) = i \int_{-\infty}^t d\tau \int_{-\infty}^{+\infty} d\bar{t} \, \vartheta(t - \bar{t}) \, E_{\alpha'k'}^-(t,\bar{t}) \mathbf{G}^>(\bar{t},\tau) E_{\alpha k}^+(\tau,t), \tag{B4}
$$

$$
\varphi_{\alpha'k',\alpha k}^{bb}(t) = -i \int_{-\infty}^t d\tau \int_{-\infty}^{+\infty} d\bar{t} \left[\vartheta(t - \bar{t}) E_{\alpha'k'}^-(t,\bar{t}) \mathbf{G}^>(\bar{t},\tau) + E_{\alpha'k'}^-(t,\bar{t}) \mathbf{G}^a(\bar{t},\tau) \right] E_{\alpha k}^+(\tau,t), \tag{B5}
$$

$$
\varphi_{\alpha'd,\alpha k}^{cb}(t) = -i \int_{-\infty}^t d\tau \int_{-\infty}^{+\infty} d\bar{t} \left\{ -\vartheta(t - \bar{t}) \left[\Upsilon_{\alpha'd}^<(t,\bar{t}) - \Upsilon_{\alpha'd}^>(t,\bar{t}) \right] \mathbf{G}^>(\bar{t},\tau) + \Upsilon_{\alpha'd}^>(t,\bar{t}) \mathbf{G}^a(\bar{t},\tau) \right\} E_{\alpha k}^+(\tau,t), \tag{B6}
$$

$$
\varphi_{\alpha'k,\alpha d}^{ac}(t) = i \int_{-\infty}^t d\tau \int_{-\infty}^{+\infty} d\bar{t} \left\{ -\vartheta(t - \bar{t}) E_{\alpha'k}^-(t,\bar{t}) \left[\mathbf{G}^<(\bar{t},\tau) \Upsilon_{\alpha d}^>(\tau,t) - \mathbf{G}^>(\bar{t},\tau) \Upsilon_{\alpha d}^<(\tau,t) \right] \right.
$$
$$
\left. + E_{\alpha'k}^-(t,\bar{t}) \mathbf{G}^a(\bar{t},\tau) \Upsilon_{\alpha d}^>(\tau,t) \right\}, \tag{B7}
$$

$$
\varphi_{\alpha'k,\alpha d}^{bc}(t) = i \int_{-\infty}^t d\tau \int_{-\infty}^{+\infty} d\bar{t} \left\{ \vartheta(t - \bar{t}) E_{\alpha'k}^-(t,\bar{t}) \left[\mathbf{G}^<(\bar{t},\tau) \Upsilon_{\alpha d}^>(\tau,t) - \mathbf{G}^>(\bar{t},\tau) \Upsilon_{\alpha d}^<(\tau,t) \right] \right.
$$
$$
\left. - E_{\alpha'k}^-(t,\bar{t}) \mathbf{G}^a(\bar{t},\tau) \Upsilon_{\alpha d}^<(\tau,t) \right\}, \tag{B8}
$$

$$
\varphi_{\alpha'd',\alpha d}^{cc}(t) = i \int_{-\infty}^t d\tau \int_{-\infty}^{+\infty} d\bar{t} \left\{ -\vartheta(t - \bar{t}) \left[\Upsilon_{\alpha'd'}^<(t,\bar{t}) - \Upsilon_{\alpha'd'}^>(t,\bar{t}) \right] \left[\mathbf{G}^<(\bar{t},\tau) \Upsilon_{\alpha d}^>(\tau,t) - \mathbf{G}^>(\bar{t},\tau) \Upsilon_{\alpha d}^<(\tau,t) \right] \right.
$$
$$
\left. + \Upsilon_{\alpha'd'}^<(t,\bar{t}) \mathbf{G}^a(\bar{t},\tau) \Upsilon_{\alpha d}^>(\tau,t) - \Upsilon_{\alpha'd'}^>(t,\bar{t}) \mathbf{G}^a(\bar{t},\tau) \Upsilon_{\alpha d}^<(\tau,t) \right\}. \tag{B9}
$$

Here, $\vartheta(t - \bar{t})$ is the step function. The EOMs for these second-tier auxiliary density matrices are as follows:

$$i\dot{\boldsymbol{\varphi}}^{aa}_{\alpha'k',\alpha k}(t) = i\boldsymbol{\varphi}^{b\dagger}_{\alpha'k'}(t) - i\boldsymbol{\varphi}^{a}_{\alpha k}(t) + \left[\gamma^-_{\alpha'k'} + \Delta_{\alpha'}(t) - \gamma^+_{\alpha k} - \Delta_{\alpha}(t)\right]\boldsymbol{\varphi}^{aa}_{\alpha'k',\alpha k}(t), \tag{B10}$$

$$i\dot{\boldsymbol{\varphi}}^{ba}_{\alpha'k',\alpha k}(t) = i\boldsymbol{\varphi}^{a\dagger}_{\alpha'k'}(t) + i\boldsymbol{\varphi}^{a}_{\alpha k}(t) + \left[\gamma^-_{\alpha'k'} + \Delta_{\alpha'}(t) - \gamma^+_{\alpha k} - \Delta_{\alpha}(t)\right]\boldsymbol{\varphi}^{ba}_{\alpha'k',\alpha k}(t), \tag{B11}$$

$$i\dot{\boldsymbol{\varphi}}^{ca}_{\alpha'd,\alpha k}(t) = \left[\gamma^-_{\alpha'd} + \Delta_{\alpha'}(t) - \gamma^+_{\alpha k} - \Delta_{\alpha}(t)\right]\boldsymbol{\varphi}^{ca}_{\alpha'd,\alpha k}(t) - i\boldsymbol{\varphi}^{c\dagger}_{\alpha'd}(t) + i\boldsymbol{B}^{<-}_{\alpha'd}\boldsymbol{\varphi}^{aa}_{\alpha'd,\alpha k}(t) + i\boldsymbol{B}^{>-}_{\alpha'd}\boldsymbol{\varphi}^{ba}_{\alpha'd,\alpha k}(t), \tag{B12}$$

$$i\dot{\boldsymbol{\varphi}}^{ab}_{\alpha'k',\alpha k}(t) = -i\boldsymbol{\varphi}^{b\dagger}_{\alpha'k'}(t) - i\boldsymbol{\varphi}^{b}_{\alpha k}(t) + \left[\gamma^-_{\alpha'k'} + \Delta_{\alpha'}(t) - \gamma^+_{\alpha k} - \Delta_{\alpha}(t)\right]\boldsymbol{\varphi}^{ab}_{\alpha'k',\alpha k}(t), \tag{B13}$$

$$i\dot{\boldsymbol{\varphi}}^{bb}_{\alpha'k',\alpha k}(t) = -i\boldsymbol{\varphi}^{a\dagger}_{\alpha'k'}(t) + i\boldsymbol{\varphi}^{b}_{\alpha k}(t) + \left[\gamma^-_{\alpha'k'} + \Delta_{\alpha'}(t) - \gamma^+_{\alpha k} - \Delta_{\alpha}(t)\right]\boldsymbol{\varphi}^{bb}_{\alpha'k',\alpha k}(t), \tag{B14}$$

$$i\dot{\boldsymbol{\varphi}}^{cb}_{\alpha'd,\alpha k}(t) = \left[\gamma^-_{\alpha'd} + \Delta_{\alpha'}(t) - \gamma^+_{\alpha k} - \Delta_{\alpha}(t)\right]\boldsymbol{\varphi}^{cb}_{\alpha'd,\alpha k}(t) + i\boldsymbol{\varphi}^{c\dagger}_{\alpha'd}(t) + i\boldsymbol{B}^{<-}_{\alpha'd}\boldsymbol{\varphi}^{ab}_{\alpha'd,\alpha k}(t) + i\boldsymbol{B}^{>-}_{\alpha'd}\boldsymbol{\varphi}^{bb}_{\alpha'd,\alpha k}(t), \tag{B15}$$

$$i\dot{\boldsymbol{\varphi}}^{ac}_{\alpha'k,\alpha d}(t) = -i\boldsymbol{\varphi}^{c}_{\alpha d}(t) + \left[\gamma^-_{\alpha'k} + \Delta_{\alpha'}(t) - \gamma^+_{\alpha d} - \Delta_{\alpha}(t)\right]\boldsymbol{\varphi}^{ac}_{\alpha'k,\alpha d}(t) - i\boldsymbol{\varphi}^{aa}_{\alpha'k,\alpha d}(t)\boldsymbol{B}^{>+}_{\alpha d} - i\boldsymbol{\varphi}^{ab}_{\alpha'k,\alpha d}(t)\boldsymbol{B}^{<+}_{\alpha d}, \tag{B16}$$

$$i\dot{\boldsymbol{\varphi}}^{bc}_{\alpha'k,\alpha d}(t) = i\boldsymbol{\varphi}^{c}_{\alpha d}(t) + \left[\gamma^-_{\alpha'k} + \Delta_{\alpha'}(t) - \gamma^+_{\alpha d} - \Delta_{\alpha}(t)\right]\boldsymbol{\varphi}^{bc}_{\alpha'k,\alpha d}(t) - i\boldsymbol{\varphi}^{ba}_{\alpha'k,\alpha d}(t)\boldsymbol{B}^{>+}_{\alpha d} - i\boldsymbol{\varphi}^{bb}_{\alpha'k,\alpha d}(t)\boldsymbol{B}^{<+}_{\alpha d}, \tag{B17}$$

$$i\dot{\boldsymbol{\varphi}}^{cc}_{\alpha'd',\alpha d}(t) = \left[\gamma^-_{\alpha'd'} + \Delta_{\alpha'}(t) - \gamma^+_{\alpha d} - \Delta_{\alpha}(t)\right]\boldsymbol{\varphi}^{cc}_{\alpha'd',\alpha d}(t) + i\boldsymbol{B}^{<-}_{\alpha'd'}\boldsymbol{\varphi}^{ac}_{\alpha'd',\alpha d}(t) + i\boldsymbol{B}^{>-}_{\alpha'd'}\boldsymbol{\varphi}^{bc}_{\alpha'd',\alpha d}(t)$$
$$- i\boldsymbol{\varphi}^{ca}_{\alpha'd',\alpha d}(t)\boldsymbol{B}^{>+}_{\alpha d} - i\boldsymbol{\varphi}^{cb}_{\alpha'd',\alpha d}(t)\boldsymbol{B}^{<+}_{\alpha d}. \tag{B18}$$

Equations (B10)–(B18) along with Eqs. (21)–(24) form a closed set of EOMs, which is established based on the novel PSLD scheme presented in Sec. II C. Such a novel TDDFT-NEGF formalism accurately characterizes the real-time dynamics of open electronic systems while preserves the positive semi-definiteness of reservoir spectral matrices.

[1] E. Runge and E. K. U. Gross, Phys. Rev. Lett. **52**, 997 (1984).
[2] K. Burke, J. Werschnik, and E. K. U. Gross, J. Chem. Phys. **123**, 062206 (2005).
[3] M. K. Casida, J. Mol. Struct.: THEOCHEM **914**, 3 (2009).
[4] R. E. Stratmann, G. E. Scuseria, and M. J. Frisch, J. Chem. Phys. **109**, 8218 (1998).
[5] X. Zheng, F. Wang, C. Y. Yam, Y. Mo, and G. H. Chen, Phys. Rev. B **75**, 195127 (2007).
[6] X. Zheng, C. Y. Yam, F. Wang, and G. H. Chen, Phys. Chem. Chem. Phys **13**, 14358 (2011).
[7] D. S. Kosov, J. Chem. Phys. **119**, 1 (2003).
[8] G. Stefanucci and C.-O. Almbladh, Europhys. Lett. **67**, 14 (2004).
[9] S. Kurth, G. Stefanucci, C.-O. Almbladh, A. Rubio, and E. K. U. Gross, Phys. Rev. B **72**, 035308 (2005).
[10] K. Burke, R. Car, and R. Gebauer, Phys. Rev. Lett. **94**, 146803 (2005).
[11] M. D. Ventra and R. D'Agosta, Phys. Rev. Lett. **98**, 226403 (2007).
[12] M. Di Ventra and T. Todorov, J. Phys.: Condens. Matter **16**, 8025 (2004).
[13] J. Yuen-Zhou, D. G. Tempel, C. A. Rodríguez-Rosario, and A. Aspuru-Guzik, Phys. Rev. Lett. **104**, 043001 (2010).
[14] A. Croy and U. Saalmann, Phys. Rev. B **80**, 245311 (2009).
[15] C. Y. Yam *et al.*, Phys. Rev. B **83**, 245448 (2011).
[16] X. Q. Li and Y. J. Yan, Phys. Rev. B **75**, 075114 (2007).
[17] X. Zheng *et al.*, J. Chem. Phys. **133**, 114101 (2010).
[18] R. Wang, D. Hou, and X. Zheng, Phys. Rev. B **88**, 205126 (2013).
[19] Y. Mo, X. Zheng, G. H. Chen, and Y. J. Yan, J. Phys.: Condens. Matter **21**, 355301 (2009).
[20] S. Chen, H. Xie, Y. Zhang, X. Cui, and G. H. Chen, Nanoscale **5**, 169 (2013).
[21] A.-P. Jauho, N. S. Wingreen, and Y. Meir, Phys. Rev. B **50**, 5528 (1994).
[22] J. Maciejko, J. Wang, and H. Guo, Phys. Rev. B **74**, 085324 (2006).
[23] Y. Wang, C.-Y. Yam, T. Frauenheim, G. Chen, and T. Niehaus, Chem. Phys. **391**, 69 (2011).
[24] R. Kosloff and D. Kosloff, J. Comput. Phys. **63**, 363 (1986).
[25] D. E. Manolopoulos, J. Chem. Phys. **117**, 9552 (2002).
[26] T. Gonzalez-Lezana, E. J. Rackham, and D. E. Manolopoulos, J. Chem. Phys. **120**, 2247 (2004).
[27] R. Baer, T. Seideman, S. Ilani, and D. Neuhauser, J. Chem. Phys. **120**, 3387 (2004).
[28] L. Zhang, J. Chen, and J. Wang, Phys. Rev. B **87**, 205401 (2013).
[29] H. Xie, Y. Kwok, F. Jiang, X. Zheng, and G. H. Chen, J. Chem. Phys. **141**, 164122 (2014).
[30] H. Xie *et al.*, J. Chem. Phys. **137**, 044113 (2012).
[31] Y. H. Kwok, H. Xie, C. Y. Yam, X. Zheng, and G. H. Chen, J. Chem. Phys. **139**, 224111 (2013).
[32] J. Hu, R. X. Xu, and Y. J. Yan, J. Chem. Phys. **133**, 101106 (2010).
[33] Y. Zhou, Y. J. Yan, and J. Shao, Europhys. Lett. **72**, 334 (2005).
[34] J. S. Toll, Phys. Rev. **104**, 1760 (1956).
[35] M. P. L. Sancho, J. M. L. Sancho, J. M. L. Sancho, and J. Rubio, J. Phys. F: Met. Phys. **15**, 851 (1985).
[36] W. H. Press, S. A. Teukolsky, W. T. Vetterling, and B. P. Flannery, *Numerical Recipes in Fortran* (Cambridge University Press, New York, 1992).
[37] E. V. Castro *et al.*, Phys. Rev. Lett. **99**, 216802 (2007).
[38] E. V. Castro, N. M. R. Peres, J. M. B. L. dos Santos, A. H. C. Neto, and F. Guinea, Phys. Rev. Lett. **100**, 026802 (2008).
[39] Z. F. Wang *et al.*, Phys. Rev. B **75**, 085424 (2007).
[40] A. Varlet *et al.*, Phys. Rev. Lett. **113**, 116601 (2014).
[41] X. Zheng, S.-H. Ke, and W. Yang, J. Chem. Phys. **132**, 114703 (2010).
[42] M. Elstner *et al.*, Phys. Rev. B **58**, 7260 (1998).
[43] C. Oppenländer, B. Korff, T. Frauenheim, and T. A. Niehaus, Phys. Status Solidi B **250**, 2349 (2013).
[44] C. Y. Yam *et al.*, Appl. Phys. Lett. **103**, 062109 (2013).
[45] C. Y. Yam, L. Y. Meng, Y. Zhang, and G. H. Chen, Chem. Soc. Rev. **44**, 1763 (2015).